Acta Crystallographica Section F
Structural Biology and Crystallization Communications
ISSN 1744-3091

Structure of an N-terminally truncated Nudix hydrolase DR2204 from *Deinococcus radiodurans*

A. M. D. Gonçalves, E. Fioravanti, M. Stelter and S. McSweeney*

Macromolecular Crystallography Group, European Synchrotron Radiation Facility, BP 220, 6 Rue Jules Horowitz, F-38043 Grenoble, France

Correspondence e-mail: mcsweeney@esrf.fr

Received 9 August 2009
Accepted 14 September 2009

PDB Reference: DR2204, 2w4e, r2w4esf.

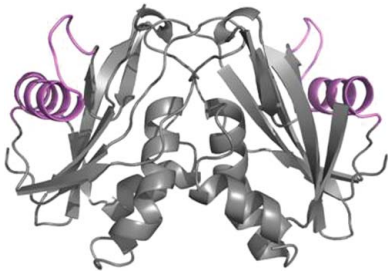

Nudix pyrophosphatases are a well represented protein family in the *Deinococcus radiodurans* genome. These hydrolases, which are known to be enzymatically active towards nucleoside diphosphate derivatives, play a role in cleansing the cell pool of potentially deleterious damage products. Here, the structure of DR2204, the only ADP-ribose pyrophosphatase in the *D. radiodurans* genome that is known to be active towards flavin adenosine dinucleotide (FAD), is presented at 2.0 Å resolution.

1. Introduction

Deinococcus radiodurans is a Gram-positive bacterium that has been shown to have remarkable resistance to ionizing radiation (Battista, 1997), in addition to an extraordinary resistance to desiccation. Analysis of the complete genome of *D. radiodurans* showed that there is a specific expansion of certain protein families; such an expansion may be connected to the organism's response to stress and damage resistance. One of the most highly represented protein families are hydrolases, amongst which are the Nudix pyrophosphatases, calcineurin-like phosphoesterases, lipase/epoxidase-like (α/β) hydrolases, subtilisin-like proteases and sugar deacetylases (Makarova *et al.*, 2000). *D. radiodurans* has 24 open reading frames (ORFs) annotated as MutT-like/Nudix hydrolases, a reasonably large number considering its proteome size (3187 protein-coding genes) and more than double the number identified for *Thermus thermophilus* (ten ORFs), an extremophile belonging to the same bacterial clade (Omelchenko *et al.*, 2005).

Nudix hydrolases are a group of phosphoanhydrases that catalyse the hydrolysis of a nucleoside diphosphate linked to another moiety *X*. Members of the Nudix family contain the consensus sequence GX_5EX_7REUXEEXGU (known as the Nudix box, where U may be Ile, Leu or Val and *X* represents any amino acid), a unique loop–helix–loop motif which forms the versatile catalytic site for diphosphate hydrolysis. The Nudix motif has been identified in protein sequences from species from all three kingdoms. Outside the conserved sequence box, Nudix-family proteins have low overall sequence identity. However, the core fold is conserved and is composed of a highly conserved $\alpha/\beta/\alpha$ sandwich, with the Nudix box sitting within a helix of the β-grasp motif. Catalytic activity takes place in the Nudix box, in which both the substrate and metal ions which are essential for activity are bound. Beyond the central fold, other regions of the sequence such as loops and the C-terminal and N-terminal regions account for substrate specificity, thus separating catalytic activity from substrate recognition and accommodation (for reviews, see Mildvan *et al.*, 2005; McLennan, 2006).

Nudix hydrolases have been termed house-cleaning enzymes, together with other enzymes such as dUTPases, ITPases and all-α nucleoside triphosphate (NTP) pyrophosphatases (Bessman *et al.*, 1996; Galperin *et al.*, 2006). They play a role in cleansing the cell pool of potentially deleterious damage products. These substrates, cell signalling molecules, regulators of cellular metabolism and metabolic intermediates, are potentially toxic compounds whose concentrations require fine modulation at different stages of the cell cycle. Typically, each enzyme may be active towards more than one nucleoside

diphosphate derivative, rendering identification of the true biological substrate a difficult task. Nudix hydrolases can process a wide variety of substrates including various ribonucleoside and deoxyribonucleoside triphosphates, nucleoside diphosphate sugar molecules, dinucleoside polyphosphates and several coenzymes including NADH, FAD and CoA. In addition, some of these enzymes have also been reported to be active towards noncanonical nucleoside triphosphates, as is the case for *Escherichia coli* MutT. The natural substrate of this Nudix hydrolase is 8-oxo-dGTP (Bhatnagar & Bessman, 1988; Akiyama *et al.*, 1989; Maki & Sekiguchi, 1992; Saraswat *et al.*, 2002), but the enzyme is also active towards non-nucleoside diphosphate derivatives such as diphosphoinositol (Safrany *et al.*, 1998) and 5-phosphoribosyl-1-pyrophosphate (Fisher *et al.*, 2002).

To date, the crystal structures of three other Nudix hydrolases from *D. radiodurans* have been reported: DR1184, DR1025 and DR0079 (PDB entries 1nqy, 1su2 and 2o5f, respectively). All three contain the conserved elements of the Nudix fold; nevertheless, substantial differences in substrate binding have been reported. DR1184 is known to be active towards CoA and has additional structural elements characteristic of the CoA-hydrolysing Nudix subfamily (Kang *et al.*, 2003). The DR1025 crystal structure showed the pivotal role of the N-terminal extension in ATP, GTP or P^1,P^4-diadenosine-5′-tetraphosphate binding and selectivity (Ranatunga *et al.*, 2004). While the biological substrate of DR0079 remains unknown, it has been proven that it is not a nucleotide triphosphate (Buchko *et al.*, 2004). Of the Nudix enzymes belonging to the *D. radiodurans* genome, DR2204 was reported to have the widest substrate specificity, being active towards ADP-ribose, GDP-mannose, FAD and NADH (Xu *et al.*, 2001) and moderately active towards dATP and dGTP. Here, we report the crystal structure of an N-terminally truncated form of DR2204 at 2.0 Å resolution.

2. Experimental

2.1. Cloning, expression and purification

The open reading frame annotated as *DR2204* was amplified by PCR from the genomic DNA of *D. radiodurans*. The PCR product comprising the 5′-CACC overhang was inserted into the expression pET151/D-TOPO directional vector (Invitrogen) following the manufacturer's recommended procedure. The resulting expression vector was used to transform *E. coli* BL21 (DE3) competent cells (Invitrogen). Transformed cells carrying pET151-*DR2204* were grown in Luria–Bertani enriched growth medium containing 100 µg ml^{-1} ampicillin; the medium was inoculated with a sample of an overnight culture and grown at 310 K until an optical density of approximately 0.6–0.7 at 600 nm was reached, at which point IPTG (isopropyl β-D-1-thiogalactopyranoside) was added to a final concentration of 0.3 m*M*, thus inducing overexpression. Cultures were allowed to grow for a further 4 h, after which the cells were harvested at 7000*g* for 20 min at 277 K and resuspended in lysis buffer [50 m*M* Tris–HCl pH 7.0, 300 m*M* NaCl, 2 m*M* β-mercaptoethanol, 5%(*v*/*v*) glycerol]. The cells were frozen at 193 K, thawed and lysed by two passages through a French press. DNase I was added to a final concentration of 20 µg ml^{-1} together with an EDTA-free protease-inhibitor tablet (Roche). The lysed culture was centrifuged at 40 000*g* for 30 min at 277 K and the soluble fraction was loaded onto a 5 ml His-Trap column (GE Healthcare) equilibrated with buffer *A* [50 m*M* Tris–HCl pH 7.5, 300 m*M* NaCl, 5%(*v*/*v*) glycerol]. The first wash consisted of a step elution to 12% buffer *B* (buffer *A* supplemented with 500 m*M* imidazole) followed by a gradient elution from 12 to 100% buffer *B*. DR2204 was eluted and pooled near 250 m*M* imidazole, as confirmed by SDS–PAGE. The pooled fractions were exchanged into a suitable buffer for His-tag cleavage by enzymatic digestion with tobacco etch virus (TEV) protease. The tag-free protein was again loaded onto a 5 ml His-Trap column and the flowthrough was collected. Further polishing was performed and oligomerization states were confirmed using a Superdex S200 HR HiPrep 16/60 column (GE Healthcare) equilibrated with 25 m*M* Tris–HCl pH 7.6, 150 m*M* NaCl, 1 m*M* DTT and 1 m*M* $MgCl_2$. The oligomerization state and monodispersity of DR2204 in solution were estimated by dynamic light scattering (Malvern Instruments, Zetasizer, Nano series).

Table 1
Data-collection statistics.

Values in parentheses are the highest resolution shell.

	Gd-SAD	Native
Beamline	ID14-4, ESRF	ID14-4, ESRF
Space group	$P4_32_12$	$P4_32_12$
Unit-cell parameters (Å)		
a	60.9	61.3
b	60.9	61.3
c	166.5	165.7
Resolution (Å)	50–2.1 (2.21–2.10)	50–2.0 (2.11–2.00)
Wavelength (Å)	0.98	0.98
No. of unique reflections	18230 (2068)	22215 (3200)
Multiplicity	15.4 (7.3)	4.4 (4.6)
Completeness (%)	95.3 (77.3)	99.7 (100)
$\langle I/\sigma(I)\rangle$	24.4 (5.5)	11 (3.6)
$R_{\rm merge}$† (%)	7.6 (24.9)	8.0 (39.1)
$R_{\rm anom}$‡ (%)	2.5 (10.6)	
FOM§	0.31	
FOM (after *DM*)	0.79	
Phasing power	1.20	
$R_{\rm Cullis}$	0.78	

† $R_{\rm merge} = \sum_{hkl}\sum_i |I_i(hkl) - \langle I(hkl)\rangle|/\sum_{hkl}\sum_i I_i(hkl)$. ‡ $R_{\rm anom} = \sum|\langle I^+\rangle - \langle I^-\rangle|/\sum(\langle I^+\rangle + \langle I^-\rangle)$. § Figure of merit.

2.2. Protein crystallization and data collection

DR2204 was successfully crystallized in two crystallization conditions using the hanging-drop vapour-diffusion method. The protein was concentrated to 16 mg ml^{-1} and mixed with an equal volume of reservoir solution containing either 0.2 *M* $LiNO_3$, 20%(*w*/*v*) polyethylene glycol 3350 (PEG/Ion Screen, Hampton Research; crystal type *A*) or 0.2 *M* KSCN, 0.1 *M* bis-tris propane pH 6.5, 20%(*w*/*v*) polyethylene glycol 3350 (PACT2 Screen, Molecular Dimensions; crystal type *B*) and allowed to equilibrate at 294 K. Crystals of tetragonal bipyramidal shape grew in 10–15 d using both crystallization conditions.

Diffraction data were collected at 100 K on beamline ID14-4 at the European Synchrotron Radiation Facility (Grenoble, France) at a wavelength of 0.98 Å. For both crystallization conditions, crystals were flash-cooled in liquid nitrogen (100 K) after soaking them for a few seconds in a solution containing a 2% increment in the precipitant and 18%(*v*/*v*) glycerol. For *de novo* phasing, a heavy-atom derivative crystal was prepared by soaking crystals of type *B* in 1 m*M* $GdCl_3$ for 18 h. Native crystals of type *A* and derivative crystals diffracted to 2.0 and 2.1 Å resolution, respectively. The solvent content was estimated as 50% based on a Matthews coefficient of 2.46 Å^3 Da^{-1} for two molecules in the crystallographic asymmetric unit and a unit-cell volume of 622 859 Å^3. Diffraction data were processed with *MOSFLM* (Powell, 1999) and further data analysis was carried out using the *CCP*4 suite v.6.0.2 (Collaborative Computational Project, Number 4, 1994). Data-collection statistics are summarized in Table 1.

Table 2
Crystallographic refinement statistics.

R_{cryst}† (%)	20.84
R_{free}‡ (%)	24.69
R.m.s.d.§ bond lengths (Å)	0.0163
R.m.s.d. angles (°)	1.583
Mean B (Å^2)	33.1
MolProbity statistics	
Ramachandran	
Most favoured (%)	96.2
Allowed (%)	3.8
Outliers (%)	0.0
Rotamer outliers (%)	1.94
Clashscore¶	1.97 (100th percentile)
Overall score¶	1.18 (100th percentile)
Overall G factor††	0.02

† $R_{cryst} = \sum_{hkl} ||F_{obs}| - |F_{calc}|| / \sum_{hkl} |F_{obs}|$. ‡ R_{free} was calculated with a small fraction (5%) of randomly selected reflections. § Root-mean-square deviation. ¶ The scores are ranked according to structures of similar resolution as formulated in *MolProbity*. †† The overall measure of structure quality from *PROCHECK* (Laskowski *et al.*, 1993).

2.3. Structure determination and refinement

The structure of DR2204 was solved by single-wavelength anomalous dispersion (SAD) from highly redundant data collected to 2.1 Å resolution from the gadolinium derivative at a wavelength of 0.98 Å. After analysing the structure factors using *SHELXC* and *SHELXD* from *HKL2MAP* v.0.2 (Sheldrick, 2008; Pape & Schneider, 2004), the position of one gadolinium site per monomer could be determined. The coordinates were then refined and phase calculations were performed using the *SHARP* suite (Bricogne *et al.*, 2003). The phases were further improved by density modification using *SOLOMON* (Abrahams & Leslie, 1996) and *DM* (Cowtan, 1999). A partial starting model was obtained by automatic model building with the program *ARP/wARP* (Perrakis *et al.*, 1999). The initial model was then completed by rounds of manual building with *Coot* (Emsley & Cowtan, 2004) and refinement with *REFMAC*. The structure of the native protein was obtained by molecular replacement with the program *Phaser* (McCoy *et al.*, 2007) using the gadolinium-derivative structure as a starting model. The native structure was refined against data collected from a crystal of type *A*, which were of better quality than the data collected from crystals of type *B*. Refinement using *REFMAC* (Murshudov *et al.*, 1997) and further cycles of manual model building using *Coot* gave a final model consisting of an N-terminally truncated form of the protein which lacked the first 55 residues in the sequence. Mass-spectrometric analysis and sequencing performed on protein crystals confirmed the protein to be truncated at this position. In both monomers the electron density is poor for a short loop between residues 149–158 and 148–159 in monomers *A* and *B*, respectively. No model could therefore be built in this region; this problem is likely to arise from disorder associated with this part of the protein. The structure was refined using bulk-solvent correction and a maximum-likelihood target function. All the data measured, apart from a 5% test set for R_{free} calculation, were used in the refinement. Side-chain atoms without visible electron density at 1.0σ were removed from the model. The quality of the structures was assessed using *PROCHECK* (Laskowski *et al.*, 1993), *WHAT IF* (Vriend, 1990) and *MolProbity* (Davis *et al.*, 2004). All residues fall within the allowed regions of the Ramachandran plot; refinement statistics and geometry analysis of the structures are summarized in Table 2.

3. Results and discussion

Full-length recombinant DR2204 was overexpressed in *E. coli* and purified to homogeneity as confirmed by SDS–PAGE. The gene

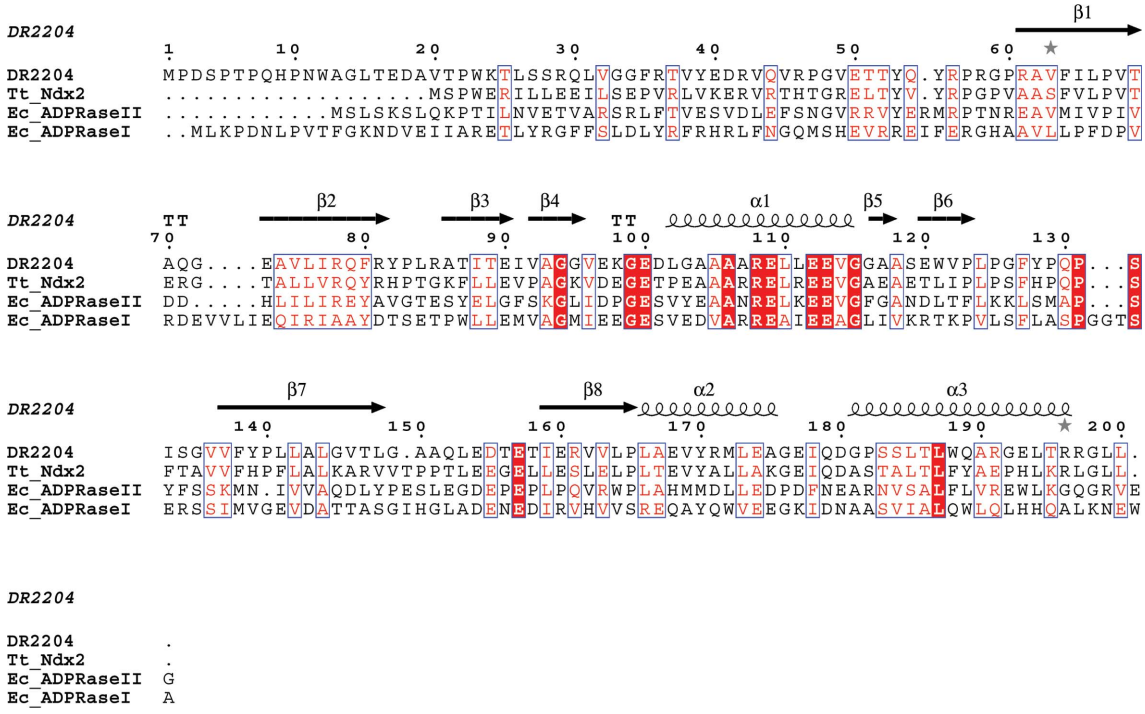

Figure 1
Sequence alignment of DR2204 with the Tt_Ndx2 (*Thermus thermophilus* HB8; 40% identity), Ec_ADPRaseII (*E. coli* ORF186; 24% identity) and Ec_ADPRaseI (*E. coli* ORF209; 21% sequence identity) proteins. Identical residues are shown in white on a red background and similar residues are shown in red on a white background. For the secondary-structure assignment, α-helices are represented as helices, β-strands are represented as arrows and β-turns are marked 'TT'. This figure was prepared with *ESPript* (Gouet *et al.*, 1999). The multiple sequence alignment was performed with *CLUSTALW* (v1.83) (Thompson *et al.*, 1994)

product corresponding to DR2204 encodes a protein of 200 amino acids with a calculated molecular mass of 21.8 kDa and a theoretical pI of 4.9. Size-exclusion chromatography indicated the presence of a homodimer in solution, a feature common to Nudix hydrolases. Dynamic light-scattering analysis confirmed the monodispersity of the purified protein.

We have determined the crystal structure of DR2204 at 2.0 Å resolution using the SAD phasing method (for data-collection and refinement statistics, see Tables 1 and 2, respectively). Both crystal types contained a homodimer in the asymmetric unit. Upon inspection of the map after density modification, no electron density was observed for about 55 residues. Inspection of maps before density modification also confirmed this observation. Further analysis of the crystal packing also suggested a lack of space to accommodate this number of N-terminal residues. Direct loading of a crystallization drop containing crystals showed a single band migrating to a molecular weight lower than 21.8 kDa. Identical drops were analysed by mass spectrometry, resulting in a spectrum dominated by a polypeptide of 15.9 kDa. N-terminal protein sequencing identified three polypeptides starting at Thr51, Tyr53 and Tyr55. The latter corresponds to a polypeptide with a calculated molecular weight of 15.8 kDa.

The crystal structure described here corresponds to an unexpected truncation of the first 55 amino acids of the N-terminus of DR2204. Based on partial proteolysis, human NUDT9, an ADP-ribose pyrophosphatase (ADPRase), was reported to have a resistant C-terminal domain which retains specific enzymatic activity while the proteolytically labile N-terminal domain enhances substrate affinity (Perraud *et al.*, 2003; Shen *et al.*, 2003). Stability studies of concentrated DR2204 in solution using SDS–PAGE analysis showed that the protein retains its molecular weight with no degradation at room temperature for over two weeks (result not shown).

The refined crystal structure of DR2204 consists of the conserved $\alpha/\beta/\alpha$ sandwich fold typical of Nudix hydrolases: the Nudix box (residues 94–115) holding the α1 helix sits between two loops accessible to the solvent, while the other two helices, α2 and α3, lie on the other side of the central β-sheet and participate in dimer-interface formation. Sequence alignment (Fig. 1) shows that DR2204 shares common characteristics with other members of the ADP-ribose pyrophosphatase (EC 3.6.1.13) subfamily, with sequence identities of as high as 24% to *E. coli* ADPRaseII (ORF186) and 21% to *E. coli* ADPRaseI (ORF209). More significantly, the overall structure of truncated DR2204 has a high identity to that of the recently solved *Thermus thermophilus* HB8 Ndx2 crystal structure (PDB code 2yvm; Wakamatsu *et al.*, 2008), with a root-mean-square deviation (r.m.s.d) of 0.73 Å for equivalent C^{α} atoms (Fig. 2*c*) and a sequence identity of 50% (40% for the full-length protein). DR2204 was found to exist as a dimer both in solution and in the crystal form (Fig. 2*a*), in contrast to *T. thermophilus* Ndx2 which crystallized with a monomer in the asymmetric unit. Despite lacking the N-terminal β-strand, which is known to domain-swap between two subunits and to offer additional interfacial area and structural stabilization in other Nudix structures

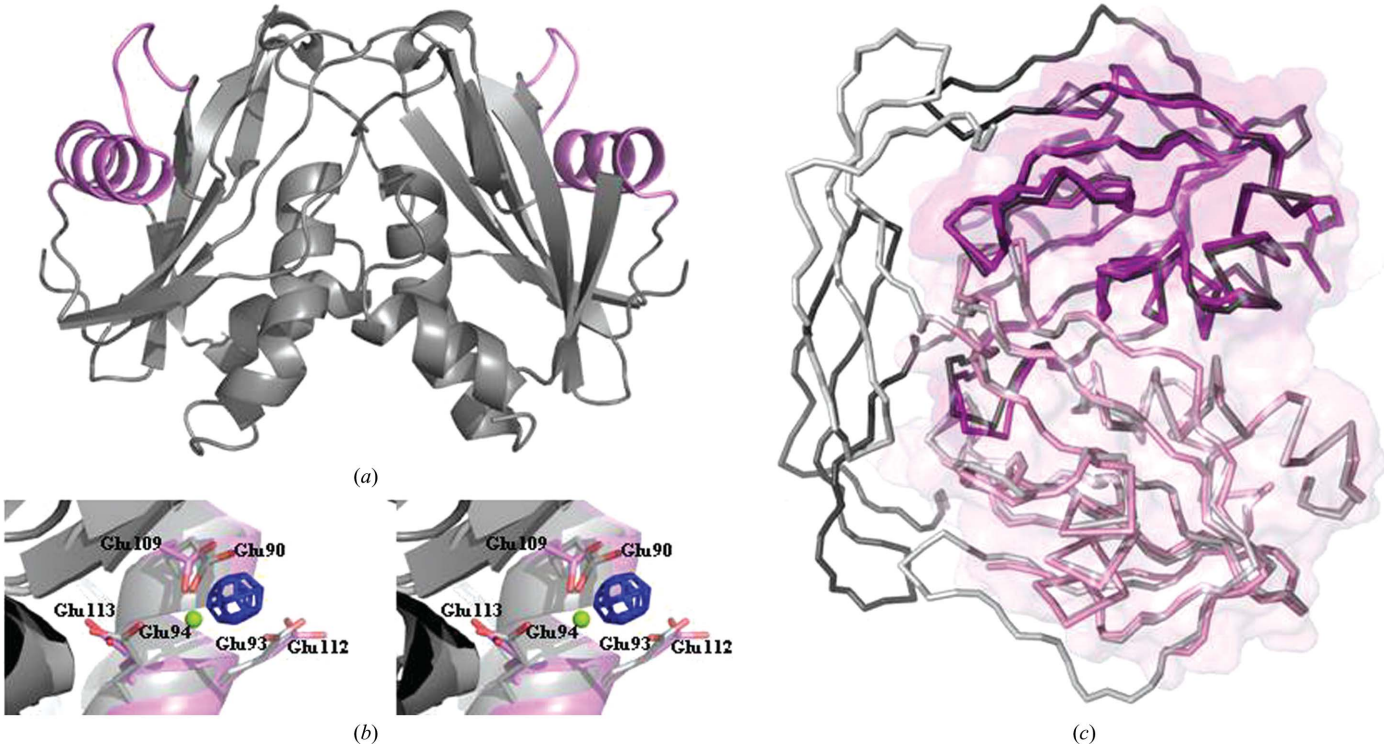

Figure 2
(*a*) The overall structure of the DR2204 dimer as observed in the asymmetric unit. The protein in grey is shown in cartoon representation, with the Nudix box highlighted in magenta. (*b*) Stereo picture showing a close-up of the Nudix box. The experimental map (blue; contoured at 10.0σ) calculated from data collected from the gadolinium-derivative crystal used for phasing is overlaid on the final model refined from data collected from the native crystal (magenta). A significant positive peak for the Gd^{3+} ion is observed in the region where Mg^{2+} is expected to bind during catalysis, between the side chains of Glu109 and Glu112. Both residues are located in the Nudix-box region, a versatile divalent metal-binding site characteristic of this family of enzymes. For clarity, the model of the ADP-ribose pyrophosphatase (Ndx2) from *T. thermophilus* (grey; PDB code 2yvm) including the Mg^{2+} 1002 ion (in green) bound to residues Glu90 and Glu94 is shown. (*c*) Superposition of DR2204 (magenta) on the structures of the ADP-ribose pyrophosphatase from *T. thermophilus* (grey; 0.73 Å r.m.s.d.; PDB code 2yvm). The surface of DR2204 is overlaid on the proteins represented in ribbon; the dimer formation buries ~1100 $Å^2$ of solvent-accessible surface. This figure was prepared with *PyMOL* (DeLano, 2003).

(Gabelli *et al.*, 2001; Yoshiba *et al.*, 2004; Wakamatsu *et al.*, 2008), DR2204 dimerized with the same orientation between the monomers, burying ∼1100 Å^2 of solvent-accessible surface (Fig. 2*a*).

Although the protein was purified in the presence of $MgCl_2$, the native structure of DR2204 was found to be in the apo form; no bound magnesium ions were found. However, using the gadolinium data and by analogy with the *T. thermophilus* Ndx2 structure, the Mg^{2+}-binding site can be identified in our structure (Fig. 2*b*). The Gd^{3+} ion is bound between the side chains of Glu109 and Glu112, thus corresponding to the magnesium ion labelled Mg2 in the *T. thermophilus* structure. In this structure Mg2 has an octahedral coordination to three glutamate residues (Glu90, Glu94 and Glu139), the α-phosphate of the bound nucleotide and two water molecules. The first two coordinating residues Glu90 and Glu94 correspond by sequence alignment to Glu109 and Glu113, respectively, in the DR2204 structure. In both human NUDT9 and *T. thermophilus* Ndx4 the metal-binding residues involve the second and fourth glutamates from the Nudix box. However, *E. coli* ADP-ribose pyrophosphatase (ADPRaseI; ORF209) also has the metal ion bound to the same corresponding glutamates as DR2204. This suggests versatility in ion binding within the Nudix box, accounting for the ability to bind both divalent and trivalent cations.

According to Xu *et al.* (2001), DR2204 is the only Nudix hydrolase in *D. radiodurans* with enzymatic activity towards FAD and NADH as well as ADP-ribose. In the *D. radiodurans* genome the Nudix hydrolase with the highest sequence identity to DR2204 is DR1007 (26% identity); however, this enzyme exhibits activity towards ADP-ribose alone, qualifying it as an ADPRaseI according to Wakamatsu *et al.* (2008). We propose DR2204 to be an ADPRaseII or rather an FAD pyrophosphatase (EC 3.6.1.18), as is *T. thermophilus* Ndx2, and possibly the only one in the entire *D. radiodurans* genome. Attempts to cocrystallize DR2204 with ADP-ribose and FAD are under way.

Mass-spectrometric analysis was performed by I. Bérard from the Laboratoire de Spectrométrie de Masse des Protéines and N-terminal protein sequencing was performed by J.-P. Andrieu from the Laboratoire d'Enzymologie Moléculaire at the Institut de Biologie Structurale, 41 Rue Jules Horowitz, 38027 Grenoble, France. AMDG acknowledges a postdoctoral research grant from Fundação para a Ciência e Tecnologia (SFRH/BEST/15939/2005).

References

Abrahams, J. P. & Leslie, A. G. W. (1996). *Acta Cryst.* D**52**, 30–42.
Akiyama, M., Maki, H., Sekiguchi, M. & Horiuchi, T. (1989). *Proc. Natl Acad. Sci. USA*, **86**, 3949–3952.
Battista, J. R. (1997). *Annu. Rev. Microbiol.* **51**, 203–224.
Bessman, M. J., Frick, D. N. & O'Handley, S. F. (1996). *J. Biol. Chem.* **271**, 25059–25062.
Bhatnagar, S. K. & Bessman, M. J. (1988). *J. Biol. Chem.* **263**, 8953–8957.
Bricogne, G., Vonrhein, C., Flensburg, C., Schiltz, M. & Paciorek, W. (2003). *Acta Cryst.* D**59**, 2023–2030.
Buchko, G. W., Shuisong, N., Holbrook, S. R. & Kennedy, M. A. (2004). *Proteins*, **56**, 28–39.
Collaborative Computational Project, Number 4 (1994). *Acta Cryst.* D**50**, 760–763.
Cowtan, K. (1999). *Acta Cryst.* D**55**, 1555–1567.
Davis, I. W., Murray, L. W., Richardson, J. S. & Richardson, D. C. (2004). *Nucleic Acids Res.* **32**, W615–W619.
DeLano, W. L. (2003). *The PyMOL Molecular Graphics System.* DeLano Scientific LLC, San Carlos, California, USA.
Emsley, P. & Cowtan, K. (2004). *Acta Cryst.* D**60**, 2126–2132.
Fisher, D. I., Safrany, S. T., Strike, P., McLennan, A. G. & Cartwright, J. L. (2002). *J. Biol. Chem.* **277**, 47313–47317.
Gabelli, S. B., Bianchet, M. A., Bessman, M. J. & Amzel, L. M. (2001). *Nature (London)*, **8**, 467–472.
Galperin, M. Y., Moroz, O. V., Wilson, K. S. & Murzin, A. G. (2006). *Mol. Microbiol.* **59**, 5–19.
Gouet, P., Courcelle, E., Stuart, D. I. & Métoz, F. (1999). *Bioinformatics*, **15**, 305–308.
Kang, L.-W., Gabelli, S. B., Bianchet, M. A., Xu, W. L., Bessman, M. J. & Amzel, L. M. (2003). *J. Bacteriol.* **185**, 4110–4118.
Laskowski, R. A., MacArthur, M. W., Moss, D. S. & Thornton, J. M. (1993). *J. Appl. Cryst.* **26**, 283–291.
Makarova, K. S., Aravind, L., Daly, M. J. & Koonin, E. V. (2000). *Genetica*, **108**, 25–34.
Maki, H. & Sekiguchi, M. (1992). *Nature (London)*, **355**, 273–275.
McCoy, A. J., Grosse-Kunstleve, R. W., Adams, P. D., Winn, M. D., Storoni, L. C. & Read, R. J. (2007). *J. Appl. Cryst.* **40**, 658–674.
McLennan, A. G. (2006). *Cell. Mol. Life Sci.* **63**, 123–143.
Mildvan, A. S., Xia, Z., Azurmendi, H. F., Saraswat, V., Legler, P. M., Massiah, M. A., Gabelli, M. A., Bianchet, M. A., Kang, L.-W. & Amzel, L. M. (2005). *Arch. Biochem. Biophys.* **433**, 129–143.
Murshudov, G. N., Vagin, A. A. & Dodson, E. J. (1997). *Acta Cryst.* D**53**, 240–255.
Omelchenko, M. V., Wolf, Y. I., Gaidamakova, E. K., Matrosova, V. Y., Vasilenko, A., Zhai, M., Daly, M. J., Koonin, E. V. & Makarova, K. S. (2005). *BMC Evol. Biol.* **5**, 57.
Pape, T. & Schneider, T. R. (2004). *J. Appl. Cryst.* **37**, 843–844.
Perrakis, A., Morris, R. & Lamzin, V. S. (1999). *Nature Struct. Biol.* **6**, 458–463.
Perraud, A.-L., Shen, B., Dunn, C. A., Rippe, K., Smith, M. K., Bessman, M. J., Stoddard, B. L. & Scharenberg, A. M. (2003). *J. Biol. Chem.* **278**, 1794–1801.
Powell, H. R. (1999). *Acta Cryst.* D**55**, 1690–1695.
Ranatunga, W., Hill, E. E., Mooster, J. L., Holbrook, E. L., Schulze-Gahmen, U., Xu, W. L., Bessman, M. J., Brenner, S. E. & Holbrook, S. R. (2004). *J. Mol. Biol.* **339**, 103–116.
Safrany, S. T., Caffrey, J. J., Yang, X., Bembenek, M. E., Moyer, M. B., Burkhart, W. A. & Shears, S. B. (1998). *EMBO J.* **17**, 6599–6607.
Saraswat, V., Massiah, M. A., Lopez, G., Amzel, L. M. & Mildvan, A. S. (2002). *Biochemistry*, **41**, 15566–15577.
Sheldrick, G. M. (2008). *Acta Cryst.* A**64**, 112–122.
Shen, B. W., Perraud, A.-L., Scharenberg, A. & Stoddard, B. L. (2003). *J. Mol. Biol.* **332**, 385–398.
Thompson, J. D., Higgins, D. G. & Gibson, T. J. (1994). *Nucleic Acids Res.* **22**, 4673–4680.
Vriend, G. (1990). *J. Mol. Graph.* **8**, 52–56.
Wakamatsu, T., Nakagawa, N., Kuramitsu, S. & Masui, R. (2008). *J. Bacteriol.* **190**, 1108–1117.
Xu, W. L., Shen, J. Y., Dunn, C. A., Desai, S. & Bessman, M. J. (2001). *Mol. Microbiol.* **39**, 286–290.
Yoshiba, S., Ooga, T., Nakagawa, N., Shibata, T., Inoue, Y., Yokoyama, S., Kuramitsu, S. & Masui, R. (2004). *J. Biol. Chem.* **35**, 37163–37174.